7-2016

Development of Nanosphere Lithography for Semiconductor Device Applications

Xing Lei
xxl9873@rit.edu

Development of Nanosphere Lithography for Semiconductor Device Applications

XING LEI

Development of Nanosphere Lithography for Semiconductor Device Applications

By

Xing Lei

A Thesis Submitted in Partial Fulfillment
of the Requirements for the Degree of
Master of Science
in
Electrical Engineering

Approved by

Dr. Jing Zhang, *Advisor* Kate Gleason Assistant Professor	Date
Dr. Sean Rommel Gleason Professor	Date
Dr. James Moon Professor	Date
Dr. Sohail A. Dianat Professor, Department Head	Date

Department of Electrical and Microelectronic Engineering

R·I·T | Kate Gleason *College of* Engineering

Rochester Institute of Technology
Rochester, New York
July 2016

Acknowledgements

I would like to thank my research partner, Matthew Hartensveld, for his quintessential effort in starting this project with me. Along with him, I thank Yu Kee Ooi, and Cheng Liu, for their assistance. I would also like to thank Kathryn King for all her help during my time at RIT.

In addition, I would like to thank Dr. Bowman, and Dr. Lu, for their engaging lectures, and introducing me to the field of devices and optics. Both have been a great influence and role model to me through my academic career at RIT.

Lastly, I thank my committee members Dr. Rommel and Dr. Moon for their time and advisement. Thank you Dr. Zhang for giving me with the opportunity to work on this project and always being available to provide me guidance.

Dedication

To my family, the Meyers, and the ones who made all of this possible.

Abstract

Nanosphere lithography, a technique of generating hexagonally packed monolayers with nanospheres, has been studied and been shown to increase the efficiency of the devices such as light emitting diodes and solar cells. In this research, the fabrication of nanosphere lithography was explored with the aim of identifying robust deposition methods. Two resultant methods yielded large (1 cm by 1 cm) monolayers of nanospheres, with further mask modification via sphere diameter reduction using reactive ion etch. Photoluminescence (PL) measurements confirmed the existence of the monolayer and the enhancement due to the addition of nanospheres. A thin layer of aluminum was deposited onto samples after performing nanosphere lithography, with the nanospheres subsequently lifted off to create various aluminum structures. Finite-difference time-domain simulations were conducted to compare with PL data. Additional experiments and processes, such as the ones that create localized surface plasmon, nano-dots, etc., are outlined for future work.

Contents

List of Figures

Chapter 1 Introduction

As society looks for more efficient lighting and energy solutions for the future, devices such as LEDs and solar cells emerge as frontrunners as they are not bounded by traditional inefficiencies and their performance can be improved tremendously. However, in order to increase their efficiency, cost-effective ways of producing nanoscale features are usually needed. One such method, namely nanosphere lithography (NSL), is not only accessible, but also economical in forming highly ordered nanoscale structures [1].

1.1 Overview of Nanosphere Lithography

Nanosphere lithography, also known by its other names such as colloidal lithography, is the creation of a monolayer of nanospheres via self-assembly. This unique property of the nanospheres can be attributed to the attractive capillary force between the nanospheres. NSL was first reported in the 1980s, with the first deposition consisting of only the drying of a colloidal solution containing nanospheres [2]. Upon further investigation, other deposition methods were developed, all with their advantages and disadvantages. The different methods are discussed extensively in the next chapter.

1.2 Overview of NSL Applications

NSL can be embedded into many applications. These not only include photovoltaic or optical devices such as solar cells and LEDs, they also include chemical and biological sensors as the hexagonal pattern from NSL can be used as the foundation for enhancement [3]. For LEDs that

function at visible wavelengths, it has been shown that even an unmodified monolayer from NSL can provide roughly 2 times emission depending on the type of nanospheres used [4]. The presence of NSs alters the effective escape cone, which becomes larger than the traditional escape cone that is only a function of the capping material, assuming the device functions in free space. GaN is often used as the capping material for LEDs and due to its high refractive index at visible wavelengths (~2.5), only ~4% of light exit out from the top of the device, which is what's perceived as effective light from the device [1]. The performance of LEDs can also be enhanced via localized surface plasmon (LSP) or surface roughening that's created by NSL patterned structures [5]. The theory behind how the spheres or LSP induces the enhancement is covered in later sections.

As for solar cells, their performance can be most directly enhanced by capturing more light, i.e., increasing absorption. NSL can be used to create various types of anti-reflection (AR) layers, which upon deposition on solar cells, increase their performance [6]. These AR layers can consist of either nano-rods, nano-cavities, or other structures.

1.3 Organization of Document

This thesis starts with a review of various aspects of nanosphere lithography and optical principles behind its applications in Chapter 2. Different methods of deposition were surveyed to not only demonstrate the progression of NSL, but also advantages and disadvantages of the methods. Then the structures that can be created by additional processing, beyond the creation of the NSL mask, are discussed to connect principles behind the improved performance to physical structures.

In Chapter 3, details of experiments that were carried out are listed along with how the experiments were characterized. Results of the experiments, including the fabrication of the monolayer, and the subsequent possessing steps, are presented and discussed along with FDTD simulations and PL measurements. Chapter 5 summarizes the work done and suggests future work in order to further implement and investigate nanosphere lithography for photonics and optical devices.

Chapter 2 Background

2.1 Nanosphere Lithography

In this section, various methods of creating the hexagonal packing mask consisting of nanospheres will be presented, and followed by the different nano-structures it can create, depending on the application it is utilized in.

2.1.1 Nanosphere Deposition

Nanosphere lithography, also referred to by its other names such as colloidal lithography, works fundamentally on its self-assembly nature. At the minimum, a drop of colloidal solution on a surface would allow the spheres to spread and self-assemble into a monolayer of hexagonal-close-packed (HCP) mask. However, the yield of such method is very low, hence the necessity to employ more effective deposition methods that are more complex [2].

Deriving from the initial deposition method, drying of colloidal solution, solvent was introduced in order to provide more control to the monolayer formation process. A mixture of solvent and NS solution would be applied onto a substrate, with the evaporation of the solvent providing the capillary force necessary for the creation of the monolayer. However, a highly temperature– and humidity–controlled environment was required in order for this method to provide a high yield as the rate of evaporation dictates the quality of the mask. In cases of uncontrolled environment, samples exhibit areas of both multilayer and monolayer deposition [7]. Other methods such as the dip-coating method, or a combination of both, that also utilizes the evaporation of solvent were investigated; however, with no substantial improvement [8].

Other mechanical ways of controlling the solvent evaporation were also attempted. Spin coating of the solvent and NS mixture would increase the evaporation rate substantially, in cases producing higher quality masks. However, most reported recipes have no theoretical backing and were all developed empirically, due to the vast number of combination of sphere concentration, type of sphere, type of substrate, and many other factors, All the factors play a role in the end result and the theoretical model of deposition has yet to be developed due to its complexity. The distinct advantage of this method is that once a mature recipe is created, it can be repeated with very little variance and can be used in large scale production [9].

Another category of deposition method involves the NSs first assembling into a monolayer prior to deposition. The colloidal mixture is first applied on top of a liquid surface, then consolidated via either mechanical or chemical compression, to aid in the formation of monolayers. The benefit of such method is that the main formation mechanism remains as solvent evaporation, and the compression only help facilitate to form even large monolayers by combining smaller monolayers [10].

Methods that only work on a particular type of substrate, such as electrophoretic deposition that requires a conductive substrate, are not discussed and only mentioned for completeness [8].

In this study of NSL, methods that don't require control over environment nor the usage of machinery were attempted. Both methods involve the NSs assembling into monolayers at the interface of liquid-air prior to deposition. Due to the absence of variability of additional

components and the robustness of the formation at the liquid-air interface, what resulted was a reliable process that produce a high quality monolayer.

2.1.2 NSL Applications

After depositing the HCP monolayer onto a substrate, various nanostructures can be obtained over an ordered array. An unmodified layer can be deposited on the top side of a LED, which has been shown to increase its overall efficiency by boosting the light extraction efficiency in the visible spectrum. Various types of NSs with different refractive indexes yield different levels of enhancement [4].

Another use of the monolayer is the production of nano-rods, or nano-wires. The mask for nano-rods can be obtained in two ways: the first one using the spheres (usually with reduced diameter), or using the cavity in between the spheres as a mask. The benefit of the first method is that the diameter of the resultant nano-rods is directly controllable by adjusting the sphere size. As for the second method, the mask can be indirectly produced by either double-masking, or by depositing a very thin layer of material, of which only a fraction would reach the substrate as most are obstructed by the nanospheres. The second method enables the fabrication of nano-rods with much smaller diameter which is desirable in some cases. By removing the undesired substrate not underneath the mask, nano-wires can be formed and be used in its intended application [11].

If the substrate removal step is not performed, the remaining structure would then be nano-dots, or nanoparticles (NPs), depending on the morphology. Due to the nature of NSL, the only polygonal NPs that can be formed are either triangular or quasi-triangular, as it is the shape of the

space in between nanospheres. Circular nano-dots, or nano-cylinder with hemisphere on top, have been reported and can be produced via either annealing the triangular nanoparticles, or using the cavity mask the NSs leave behind after lift off. These such NPs are used in producing localized surface plasmon with different types of metal, most popularly Ag, for enhancing the visible spectrum [12,13].

2.2 Optical Concepts

Several optical concepts that are pertinent to the next few chapters are introduced and briefly discussed in this section to aid in understanding of the effects of NSL and subsequent structures.

2.2.1 Light Extraction Efficiency

Two parameters dictate the overall efficiency of a LED: its internal quantum efficiency, which is the product of injection efficiency and radiative efficiency, and its light extraction efficiency (LEE). The first one pertains to the ratio of photons generated to electrons through the device, whereas the second one is the ratio between the number of photons generated versus the number of photons that escape the device. For this study, the emphasis would be on the latter as the addition structures on top of the sample substrates would only alter the LEE. Due to the high refractive index of GaN, a commonly semiconductor material used as a capping layer of LEDs, most of the light generated from the device remained trapped in such layer. Per Snell's law, the critical angle can be calculated by (2.1) where n_1 and n_2 are the refractive index of GaN and air

respectively, with θ_1 and θ_2 being their corresponding angles. At θ_2 equals 90°, θ_1 becomes the critical angle at which point total internal reflection occurs.

$$n_1 \sin(\theta_1) = n_2 \sin(\theta_2) \tag{2.1}$$

Assuming a refractive index of ~2.5 for GaN in the visible spectrum, the critical angle is calculated to be 23.6°. Using a point source, the fraction of power that device effectively outputs can be calculated by finding the ratio of the surface area of the cap of such cone, and the surface area of a sphere with equivalent radius. This specific derivation, done by Ee, also involved a Taylor series approximation to simplify resultant expression [1]. After a two term Taylor series approximation (which is appropriate due to the small angle), the expression becomes (2.2), which calculates the power ratio to be 4% when GaN is used as the capping layer of the LED.

$$\frac{P_{escape}}{P_{source}} \cong \frac{1}{4}\left(\frac{n_{air}}{n_{GaN}}\right)^2 \tag{2.2}$$

Thus, an increase of the effective critical angle would be equivalent to increasing the surface area of the cap of the cone, resulting in more emission and an increased performance of the LED. The layer of nanospheres effective decreases the Fresnel reflection that occurs within the cone, as well as providing other paths for light to escape outside of the cone, increasing the device's efficiency [14].

2.2.2 Localized Surface Plasmon

Localized surface plasmon resonance (LSPR) is a phenomenon that induces electromagnetic-field enhancement and it occurs when an electric field of the resonating frequency hits a metal nanoparticle, creating localized surface plasmon (LSP) [15]. LSPR has been utilized in

order to increase the radiative efficiency of LEDs, with Ag and Au in the visible spectrum, and Al in UV [16]. As it is not essential to this particular experiment and merely one of the possible applications for NSL, a thorough theoretical behavior of such phenomenon is not presented here and is substituted with a presentation of the general understanding of why and how it occurs.

As an electric field comes in contact with the metallic nanoparticles, it would cause the electrons inside the metal to respond in return. When the electric field interacts with the NPs at the resonance frequency, the electrons, although still bounded by the metal NP, oscillate in response. This resonance frequency is a function of many things, including not only the type, size, and shape of the metal NPs, but also the environment it is in. Due to this unique property, LSPR is not only used for optical applications for its obvious enhancement and specific wavelengths, but it's also used for biological and chemical sensing where it can be fine-tuned to detect a specific chemical or molecule [17,18]. LSPR provides many more degrees of freedom than its closely related counterpart, surface plasmon resonance, as the latter is mostly based on a structure of thin metal film, versus metal NPs.

It has been demonstrated that utilizing LSPR, polygonal aluminum NPs can enhance deep UV spectrums by factors of greater than 5. Utilizing NSL, NPs of different metal and sizes can be created in a patterned order, which will enable further investigation of LSPR [16].

Chapter 3 Experiment

In this chapter, the experimental procedure and details are presented, first with the formation of the PS sphere monolayer, then the transfer of monolayer, and subsequently manipulation of the sphere sizes. Metal is then deposited and finally followed by the lift-off procedure for the purpose of producing surface plasmon and other nanostructures.

3.1 Experimental Setup

PS spheres from two sources, Polyscience, and Bangs Laboratory, were used in experiments. The sphere solution from Polyscience was purchased in the form of water solution with 2.5% wt. spheres of nominal diameters 500 nm and 750 nm; the sphere solution from Bangs Laboratory is in the form of 10% wt. solution with diameter of 320 nm. All spheres are functionalized with carboxyl groups for the purpose of forming the hexagonal packing pattern. For the experiment, various concentrations of solutions were created via either centrifugation or dilution. The time necessary for centrifugation is calculated via (3.1), where V is velocity in cm/sec, G is G force in cm/sec^2, ρ_1 and ρ_2 is the density of the particle and suspending media respectively, both in g/cm^3, n is the coefficient of viscosity in g/cm-sec, and a is the radius of the NS. For PS spheres submerged in water, the values for ρ_1 is 1.05 g/cm^3 and n is 1.002 g/cm-sec. The calculated time is used to ensure no over-centrifugation occurs, and the sphere pellet formed at the bottom can be reintroduced to the final solution without issue [19].

$$V = \frac{2Ga^2(\rho_1 - \rho_2)}{9n} \tag{3.1}$$

Various concentrations, 2.5%, 5% and 10% were used in the experiment. The sphere solutions were mixed with equal parts of ethanol, which serves the purpose of helping the spheres spread during the formation of the monolayer, prior to usage.

In order to produce the monolayer, a glass slide pretreated with 10% SDS by soaking for a minimum of 24 hours prior is necessary. Two methods were used in the experiment with equal amount of success. For the first method, the pretreated glass slide is rinsed thoroughly with DI water and dried with nitrogen, then lowered and set in a 6-inch diameter beaker filled with 150 ml of water at an angle no greater than 45 degrees with the bottom of the beaker, with a portion above the surface. Then using a micropipette, the solution with equal parts of ethanol is applied to the glass slide slowly, ensuring a gradual introduction to the water surface. The SDS treatment would ensure the sphere solution does not stick to the glass slide but rather spread to its edges. As the sphere solution hits the water surface, the monolayer is formed [20].

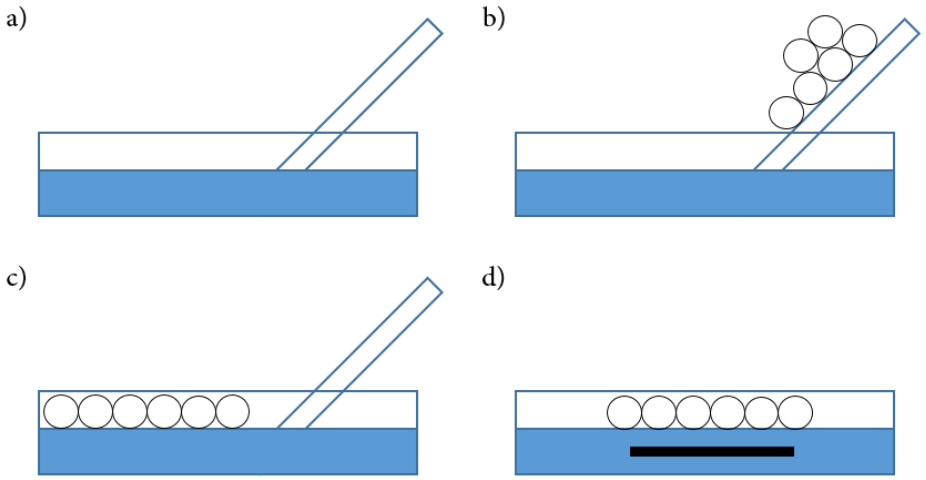

Figure 1 – Visual illustration of deposition method 1: a) set glass slide at small angle to surface, b) apply sphere solution onto glass slide, c) formation of monolayer, d) lift monolayer using substrate underneath.

For the second method, the glass slide is rinsed and dried in a similar manner as above, then laid down in a beaker. Then DI water is introduced to the beaker around the glass slide, until the glass slide is completely surrounded and the water almost flowing over the top. The sphere solution is then applied to the glass slide, and it would spread to the water forming the monolayer. The water level is then raised by pumping more water to the bottom of the beaker using an ordinary pipette, while ensuring not to disrupt the monolayer on top [10].

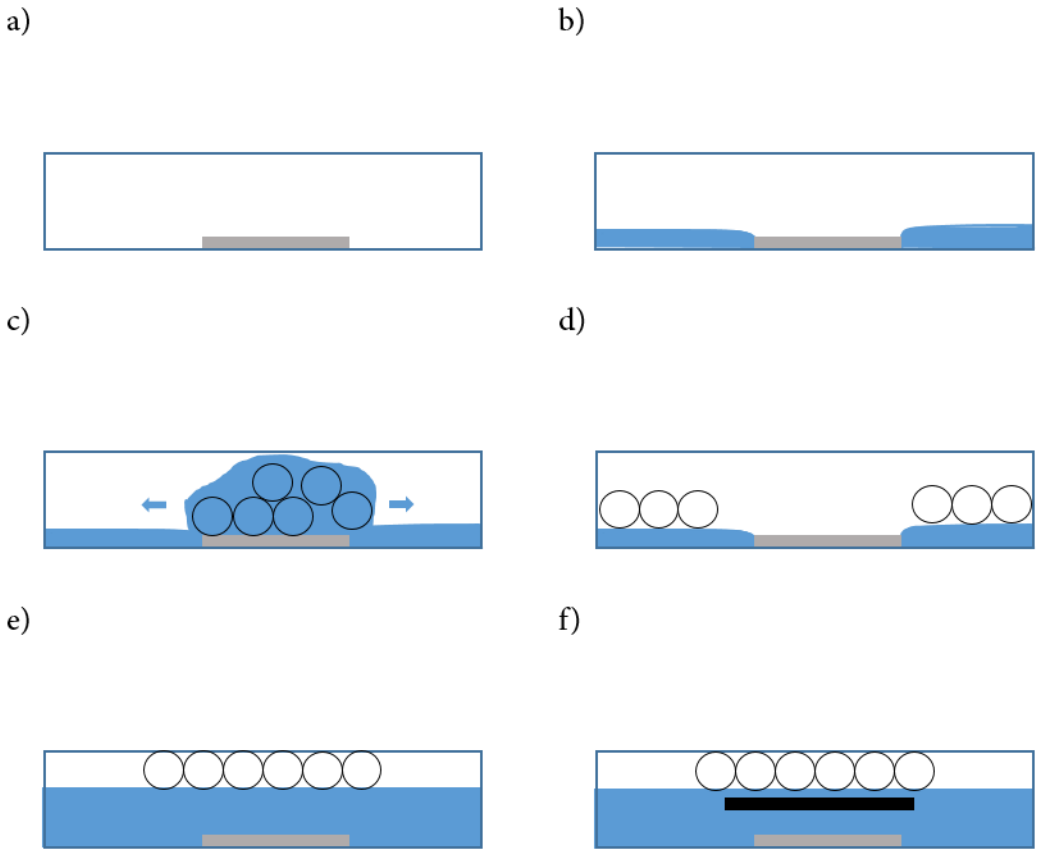

Figure 2 – Visual illustration of deposition method 2: a) set glass slide flat in empty container, b) fill water to glass slide edge, c) apply sphere solution to glass slide, d) formation of monolayer on water surface, e) raise water level, f) position substrate underneath monolayer and lift.

For both methods, the amount of water is arbitrary as long as a sufficient height is achieved to allow easy transfer of monolayer to a substrate. The same applies to the amount of sphere solution depending on the size of the container used; a reference amount of ~20 μl can be applied as a starting point.

After the formation of monolayer on top of the water, if the size of individual monolayers are too small, a few drops of 2% SDS can be applied to chemically compress the monolayers together by altering the surface tension, or alternatively a physical barrier, such as a glass slide, can be used to mechanically compress the monolayers together. The monolayers can also be combined by applying gentle oscillatory motion to the container [8].

3.2 Nanosphere Deposition

3.2.1 Deposition on Silicon

Similar to the glass slide, in order to increase the hydrophilicity of silicon, the substrates need to be pre-treated in the same manner, then rinsed and dried with nitrogen prior to performing the nanosphere deposition. The monolayers formed via one of the two methods above can be visibly seen on top of the water surface, with the color depending on the diameter of the spheres used. After confirming the presence of the monolayers, the silicon substrate can be submerged into the container, then positioned underneath the monolayer, and lifted up to transfer the monolayer to the sample.

3.2.2 Deposition on GaN

Unlike silicon, the chemical surface treatment using SDS is ineffective in increasing the hydrophilicity, and an oxygen plasma is used in place to create the same effect. A Drytek 482 Quad Etcher is used to treat the GaN substrates for 600 seconds, with a RF power of 300 W, at an oxygen flowrate of 100 sccm, with the pressure being 200 mTorr. After treatment, the GaN substrate can be used in the same manner as the silicon substrate to lift up the nanosphere monolayer [21].

3.3 Sphere Diameter Reduction

The reduction of sphere diameter can be achieved via reactive ion etch, using the Drytek 482 Quad Etcher in this particular case. The recipe is a derivation of the recipe used as reported by Brown and has the settings of a RF power of 75 W, 200 mTorr, an oxygen flowrate of 200 sccm for various amount of time depending on the desired diameter reduction. For complete detachment of individual spheres from each other, a reduction of no less than ¼ of the original diameter is recommend as "necking", spheres remain connected to each other even after RIE, occurs otherwise [9].

3.4 Metal Deposition

Metal deposition is performed using the CHA Ebeam Evaporator. Aluminum was deposited onto both silicon and GaN substrates secured via tape described above. A pressure of 8 μTorr was used and the thickness of aluminum was roughly 18 nm. The deposited thickness of any material has to be less than half of the reduced sphere diameter to guarantee complete removal of PS spheres for the lift off process.

3.5 Lift Off Procedure

For the removal of PS spheres, a cotton swab soaked with acetone can be applied to the substrates gently. The complete removal of spheres can be confirmed by comparing the substrates with a pristine sample without nanosphere lithography performed. Additionally, the samples can go through an ultrasonic bath in acetone to ensure complete removal of all the spheres [9].

3.6 Characterization

Three different tools are used for characterization in this experiment. The first one is the Leica Inspection Station, an optical microscope, with up to x100 objective. The images taken with the station are all accompanied with its scale bar in the bottom right corner. The second one is a Toshiba SEM for higher resolution images, with the voltage being at either 5 kV or 10 kV, which is indicated in the images. The third one is a photoluminescence (PL) system that consists of 325 nm He-Cd laser at ~33 mW, with a Horiba Syncerity detector setup as Figure 3. The laser can either be pumped from the front, or the back of the sample, depending on how the sample is mounted. The side that the laser comes in contact with first is considered to be the side that it is being pumped from.

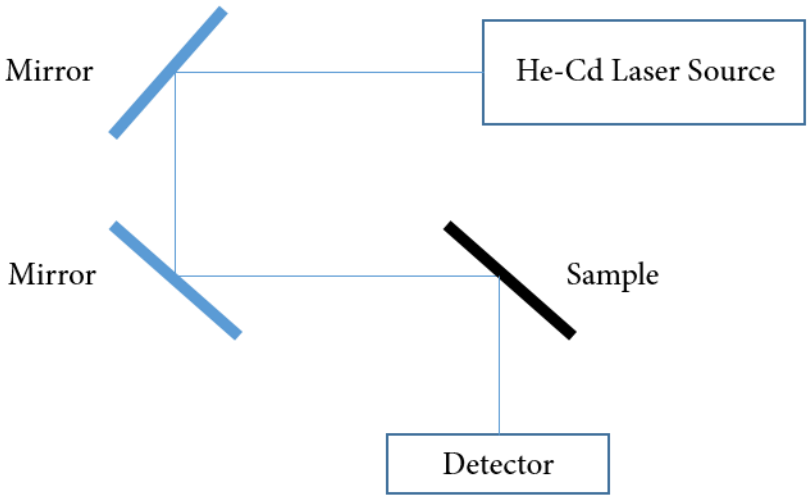

Figure 3 – PL system setup.

Chapter 4 Experimental & Simulation Results

In this chapter, the results obtained from previous chapter's experimental procedure are presented. This is followed by various finite-difference time domain simulations from RSoft, then PL measurements for comparison and discussion [22].

4.1 Experimental Results

Results of nanosphere lithography with varying parameters (such as the concentration of the solution used, method of deposition, *etc.*) are described step by step below.

4.1.1 Deposition on Silicon

By applying a mixture of several μl (less than 10 μl) of 1:1 ethanol and 2.5% 750 nm diameter sphere solution to a 5-inch diameter beaker then subsequently attempting to transfer the monolayer to a silicon substrate, the result is captured Figure 4. There is very little coverage, with isolated spheres or forming small islands, and no large areas of hexagonal packing monolayers. The low concentration of nanosphere causes them to sink into the water, rather than remaining on top of the surface of the water. The same experiment was repeated with the exception of drying the sample on a hot plate (Figure 5) below the melting temperature of PS spheres at 40 °C for 10 to 20 minutes, with no improvement.

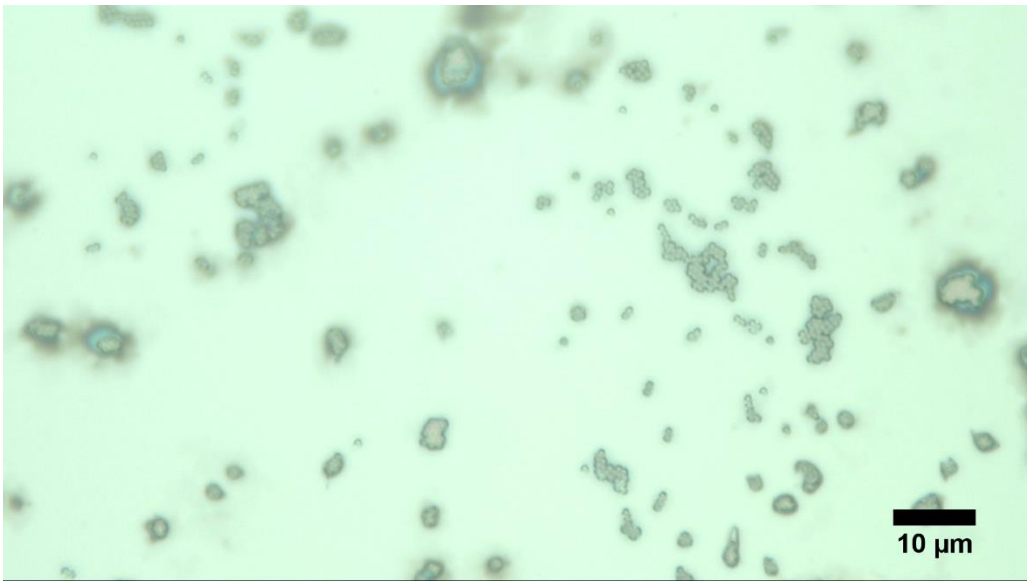

Figure 4 – NSL with 2.5% sphere solution on silicon, air dried.

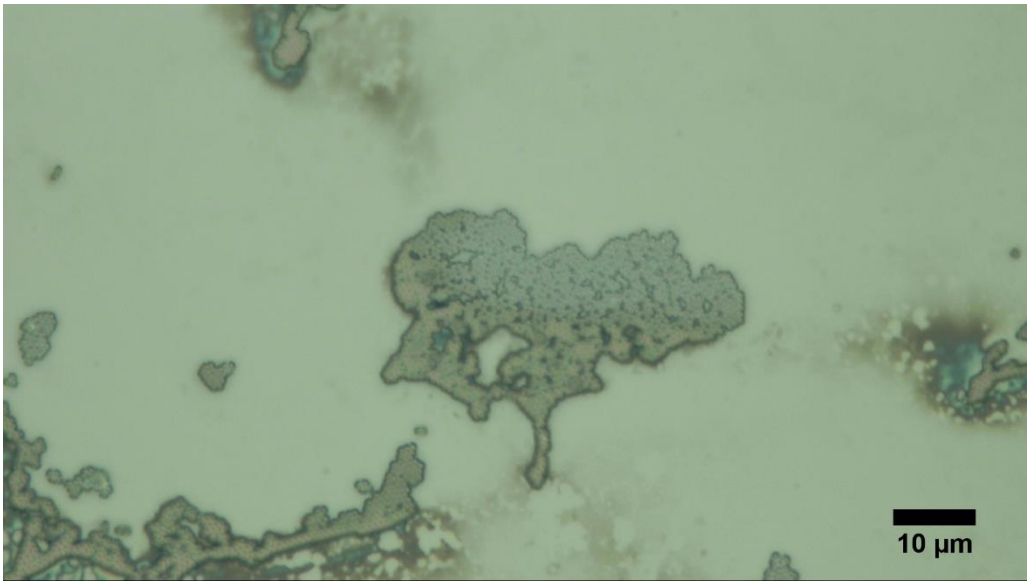

Figure 5 – NSL with 2.5% sphere solution on silicon, dried on hot plate.

In order to increase the coverage, a larger amount of solution (upwards of 800 µl) was applied, yielding results in Figure 6. The hexagonal packing monolayers are clearly visible in certain areas, while others were void of spheres, as shown in Figure 6.

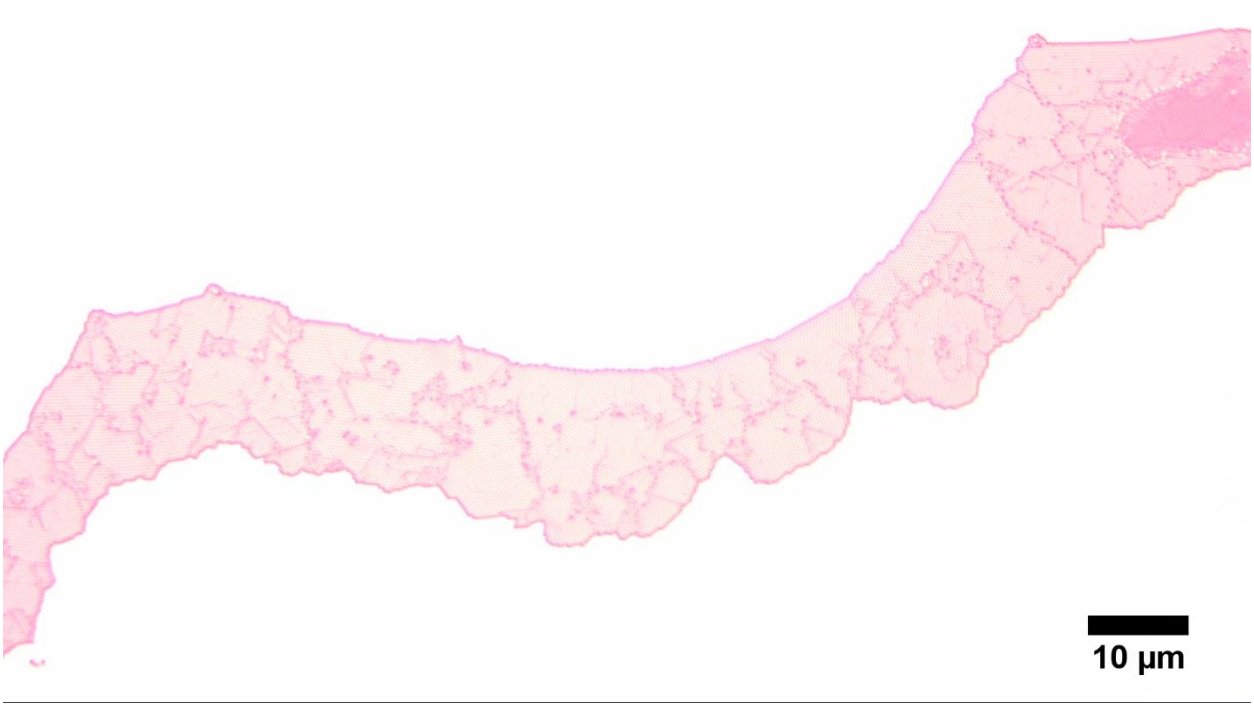

Figure 6 – NSL with 2.5% 800 µl sphere solution on silicon.

A more intensive investigation of the effect of increased density of spheres, relative to the surface area of the container was then conducted. Substituting the container with one that is 1.5-inch in diameter, and vastly increasing the amount of solutions yielded greater coverage; however, areas with multiple monolayers on top of each other or isolated nanosphere on top of the monolayer, which is undesirable, also started to form (Figure 7). The produced monolayers did not cover the substrate uniformly, as seen in Figure 8, and they have the distinct island-like shapes that are heavily influenced by the direction of how the solution dried after the monolayer has been scooped up.

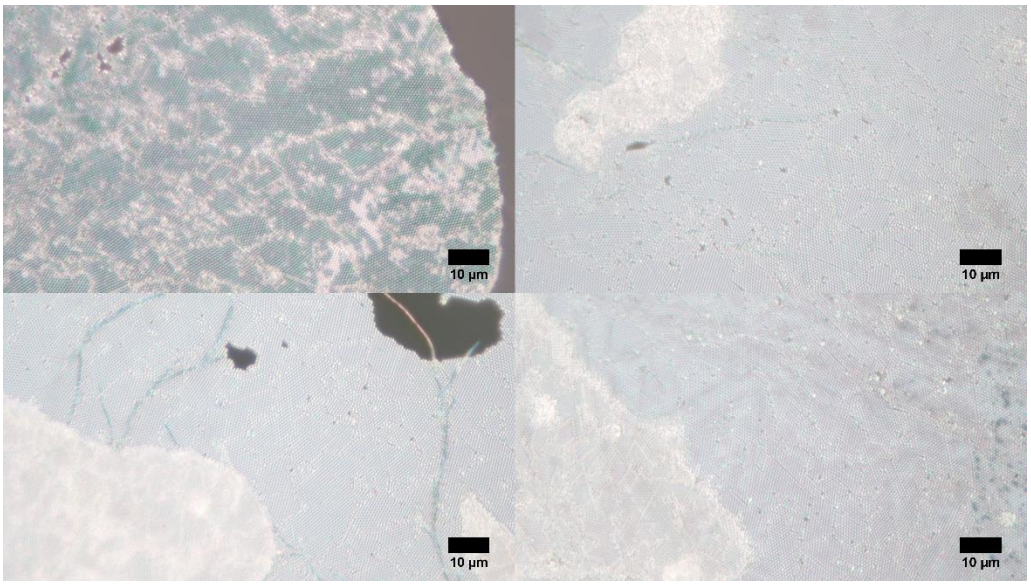

Figure 7 – NSL with various amount of 2.5% sphere solution, in clockwise order from top left: 0.9 ml, 1.8 ml, 3.6 ml, and 4.6 ml.

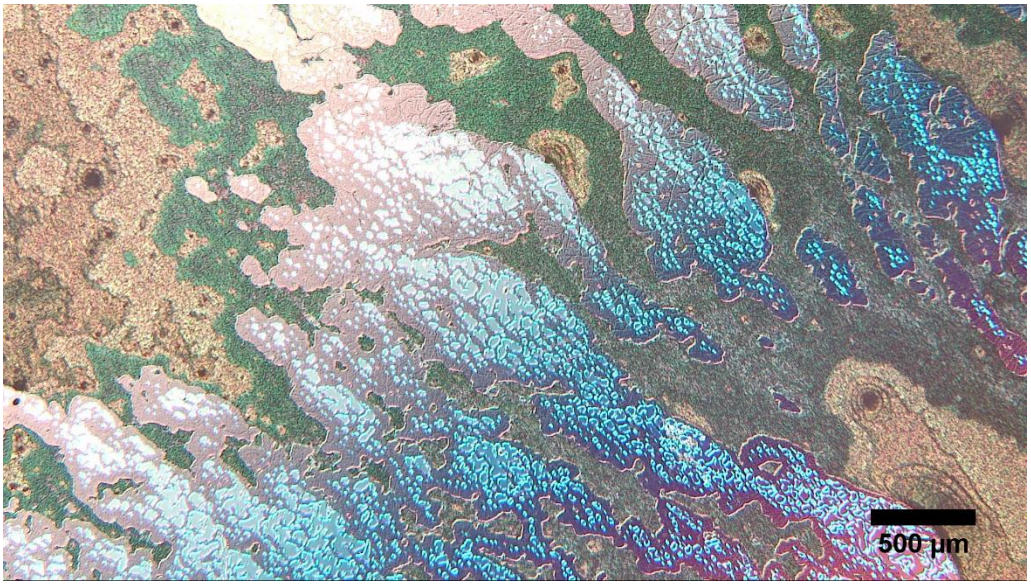

Figure 8 – NSL with 4.6 ml of 2.5% sphere solution at x2.5 objective. The different colors signify different number of layers.

To improve the uniformity of the nanosphere deposition, ~10% sphere solution (created by the centrifugation steps described in previous chapter) is used in place of the 2.5% sphere

solution, in the 1:1 mixture with ethanol, with the sphere diameter being 500 nm. Upon the mixture being applied to the glass slide, the monolayers, indicated by their diffractions, can immediately be seen on top of the water surface. The silicon substrate was then manually positioned underneath and scooped up the visible monolayers. The resultant deposition can be seen in Figure 9. Although not shown in the picture, the monolayer extends out beyond the image and is roughly 1 cm^2. In Figure 10, the monolayer can be seen to have very few nanospheres on top of it, unlike in Figure 7. However grain boundaries, due to different orientations of the individual monolayers, are still visible, along with the existence of point defects. The total volume of the ethanol and nanosphere mixture used ranged from 20 to 80 μl, depending on the container used.

Figure 9 – NSL with ~10% sphere solution on silicon, the visible lines signifies grain boundaries within the monolayer.

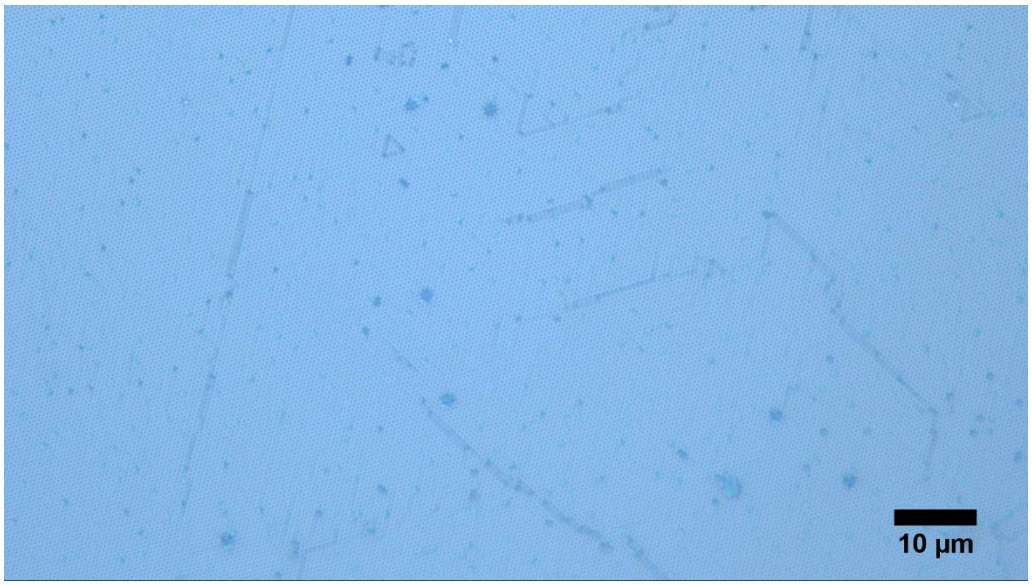

Figure 10 – a large monolayer with point defects and grain boundaries.

The same coverages were obtained while using a 5% sphere solution with 320 nm diameter spheres. The resultant monolayers exhibit similar grain boundaries and point defects. The samples, with different diameter spheres, were all characterized using a SEM in Figure 11 – Figure 13, confirming the hexagonal packing structure, and the existence of various defects.

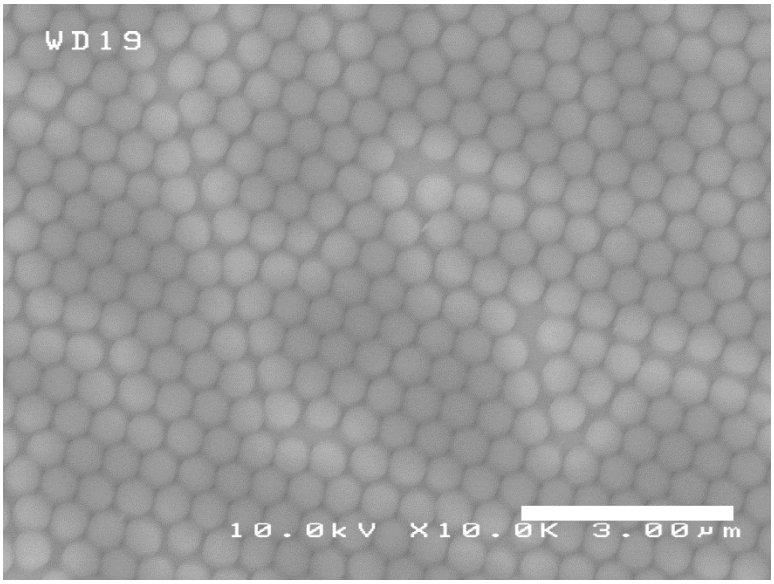

Figure 11 – Monolayer with sphere diameter of 500 nm.

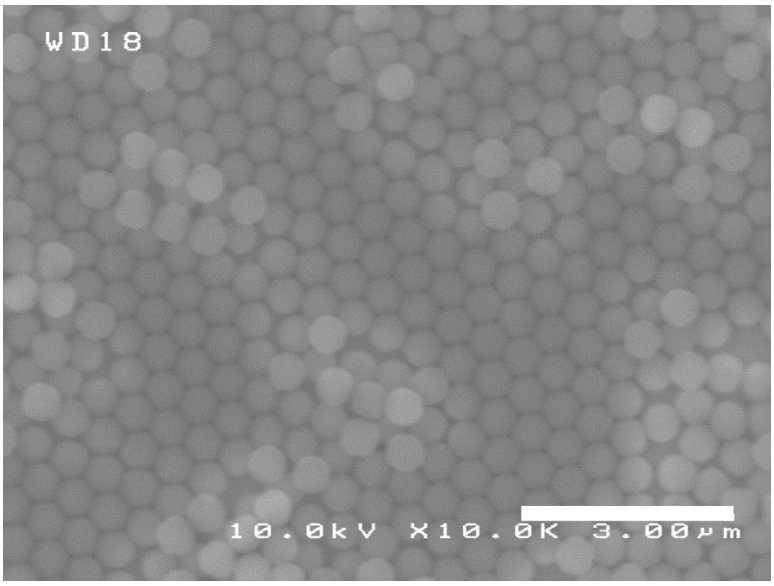

Figure 12 – Monolayer with defects.

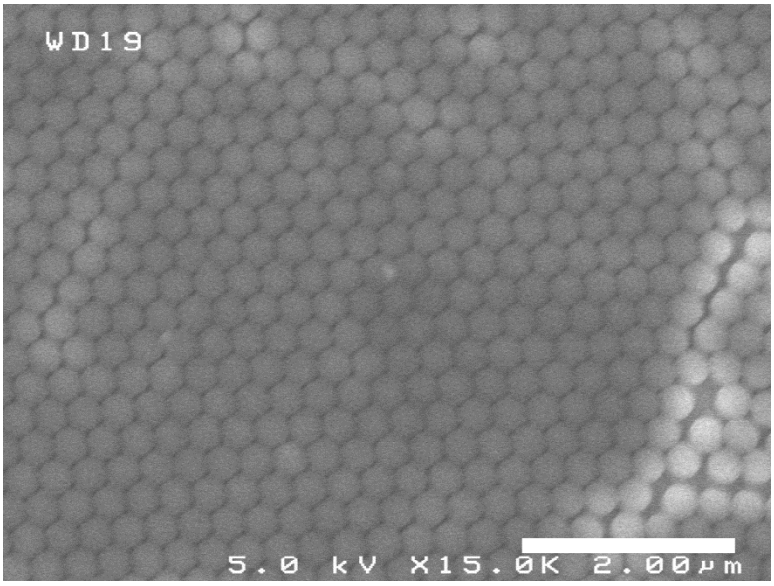

Figure 13 – Monolayer with 320 nm diameter spheres

4.1.2 Deposition on GaN

In order to perform NSL on GaN samples, the plasma treatment described in the previous chapter was used to increase the hydrophilicity of the surface. There was a distinct visible difference in its hydrophilicity as the treated samples retained significantly more water on their surface than

untreated samples, after dipping the samples into water. After the treatment, the same deposition procedure was performed with the modified substrate. Figure 14 captures nanospheres on GaN substrate. The blurriness in the image can be attributed to the transparent property of the sample and thus making it more difficult to image. The right half of the image demonstrates the hexagonal packing monolayer, whereas the left half portion demonstrates the unordered packing of nanospheres that form due to the solution drying on the substrate. A point defect due to abnormally large nanosphere is also captured.

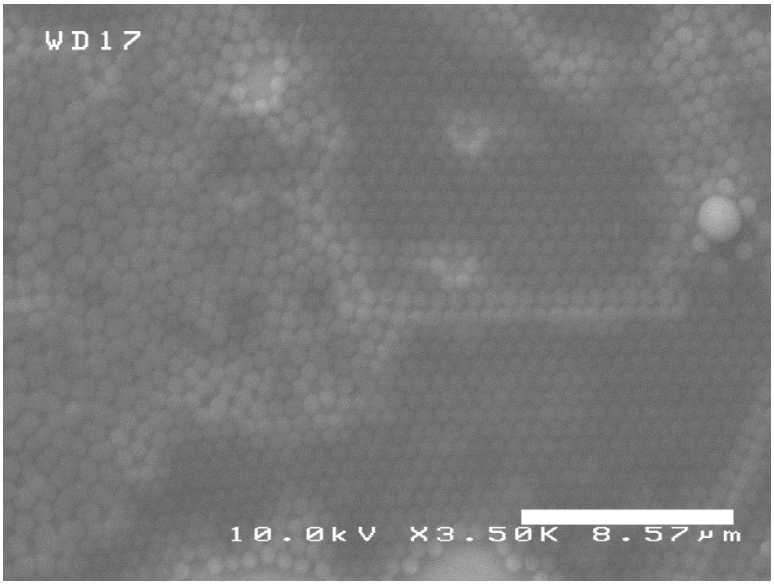

Figure 14 – NSL on GaN

4.1.3 Post Deposition Processes

After deposition, the samples underwent RIE to reduce the sphere diameters while the spacing between the spheres, which was set by the original diameter, remained the same. The recipe (with and without 6 sccm of CF_4) were used on two different diameter spheres, yielding different etch rates. The different etch rate is more likely contributed to the difference in sphere diameter

(500 nm vs. 320 nm), than the presence or absence of CF_4. Figure 15 consists of post-etching SEM images of 500 nm diameter spheres that underwent 12 seconds and 36 seconds of etching respectively.

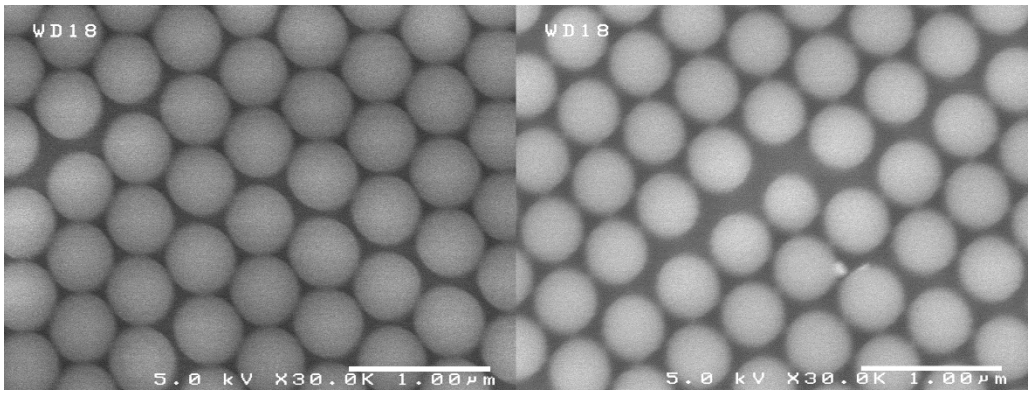

Figure 15 – 12 seconds (left) and 36 seconds (right) of RIE with 500 nm diameter spheres.

The same recipe without the CF_4 flow was performed on 320 nm nanospheres for 23 seconds and 45 seconds respectively, with the results captured in Figure 16. The trends are plotted in Figure 17, with etch rates of roughly 1.7 nm/s and 4 nm/s for the two trials with different spheres. The above etched rates were extrapolated linearly, which is only representative of etching that does not involve significant size reduction of the spheres. As shown in the etched trend for the 320 nm diameter sphere in Figure 17, the second ~23 seconds reduced the diameter much more than the initial 23 seconds of etching, which is in line with what was reported previously, and made sense as the reduction in volume does not correlate linearly with reduction in diameter[24].

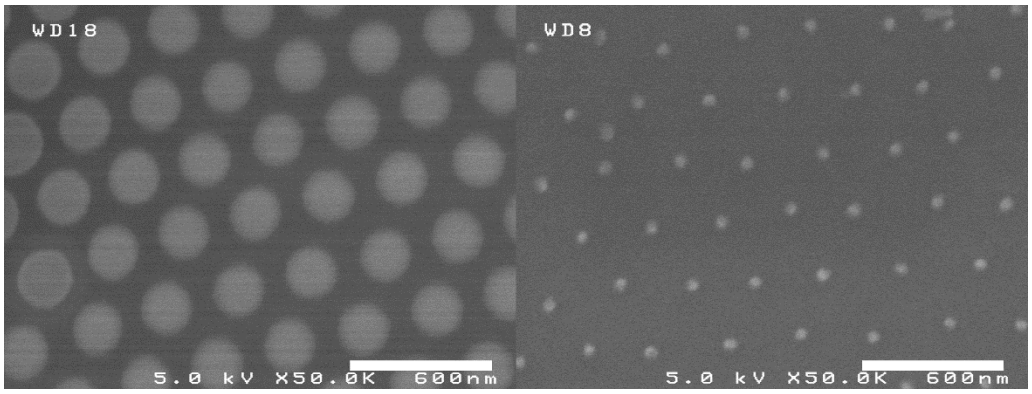

Figure 16 – 23 seconds (left) and 45 seconds (right) of RIE with 320 nm diameter spheres

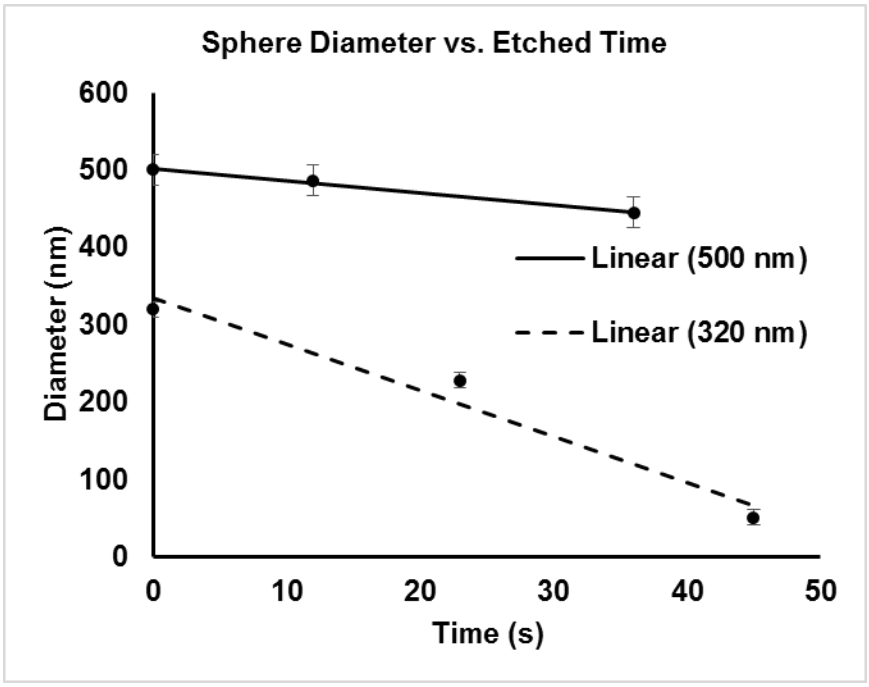

Figure 17 – Trend of sphere diameter vs. etched time.

After reducing the diameter of the spheres, a layer of aluminum was deposited. The samples were characterized again after the spheres were lifted off. Figure 18 demonstrates an aluminum (the lighter regions) structure with hexagonally packed cavities on top of silicon (the darker circles). The images were captured at a lower voltages (2-5 kV) to take into account the presence of aluminum.

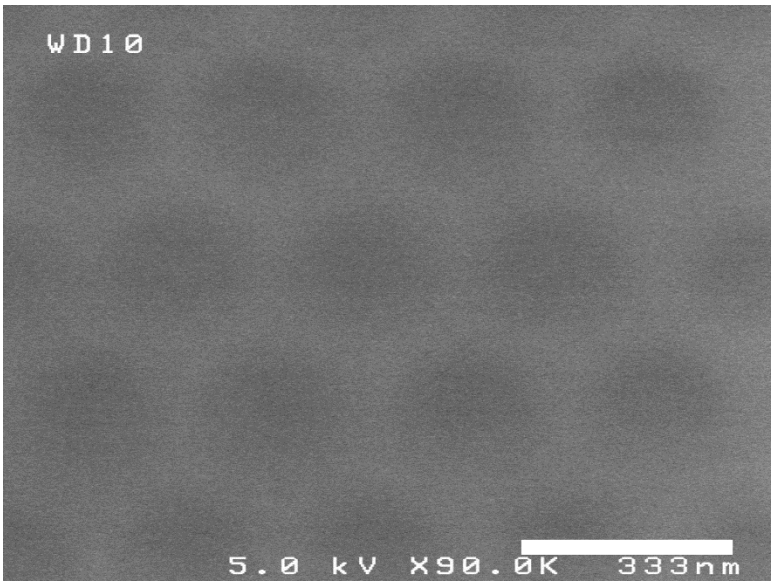

Figure 18 – Aluminum structure on silicon [24].

Aluminum was also deposited onto the sample with significantly reduced diameter (~50 nm), with the results captured in Figure 19. The hexagonal packing pattern remains, with much smaller cavity this time. The image also captured several irregularities in the mask, such as the bottom left corner, with what appears to be a sphere that remained in its place after lift off.

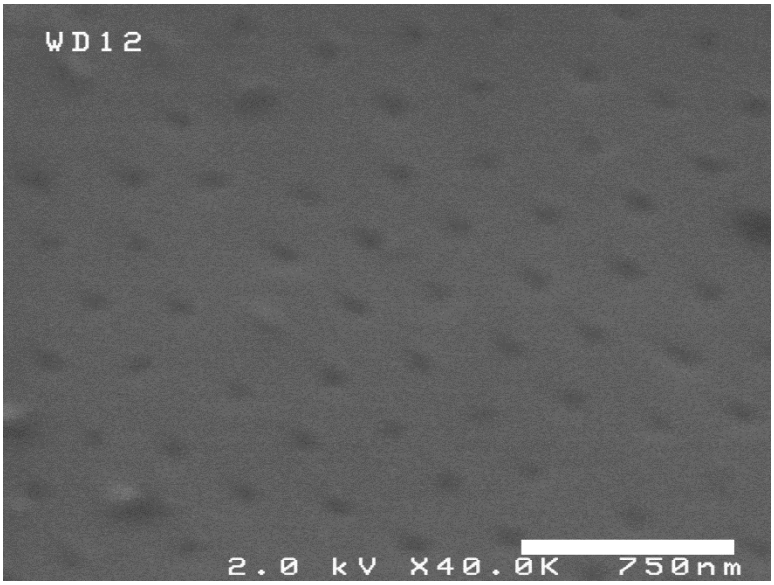

Figure 19 – Aluminum structure with small cavities on silicon [24].

This defect was also present in other locations of the samples. A defective area is captured in Figure 20. There seemed to be residues of either polystyrene or aluminum on top of polystyrene spheres. This issue can be traced down to two primary causes, the first one being the quality of the mask, where this location could previously be a location of multiple monolayers on top of each other; and the second cause being the polystyrene spheres weren't successfully removed during the lift off procedure. The first cause can be minimized by creating a higher quality mask, with minimal regions of multi-layer, and the second cause can be minimized by using an acetone ultrasonic bath to remove the spheres at locations the lift-off procedure isn't effective.

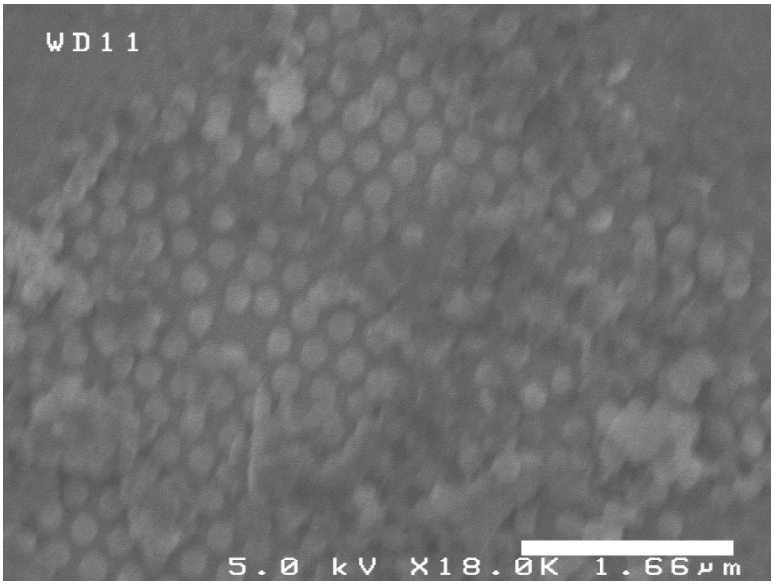

Figure 20 – defective area after aluminum deposition and lift off [24].

To produce LSPs, a layer of aluminum was also deposited on top of the monolayer on GaN that is grown on single side polished sapphire, with no sphere diameter reduction. Different than the aluminum structures already presented (completely connected with nano-cavities), in order to obtain LSP, the deposited aluminum must be discrete nanoparticles.

4.2 Simulation Results

In this section, results from FDTD simulation, using RSoft, are presented to demonstrate the effect of not only the PS sphere mask created by NSL, but also LSPs. Various parameters were swept to provide more insight as to how the various hexagonal patterns alter the spectrum of GaN on sapphire in this particular case differently.

All simulations were ran with the following parameters, unless specified otherwise: uniform grid of 0.02 μm in *x, y*, and *z*; free space wavelength of 370 nm (roughly the peak of GaN); perfectly matched layer (PML) on all sides, with thickness of 0.2 μm (10 times grid size); *x* and *y* dimensions are both from -5 μm to 5 μm, *z* dimension is from 0 to ~0.8 μm, with minor changes depending on the radius of the spheres. The refractive index of sapphire was set to be 1.79, with its thickness set to 0.2 μm, and the refractive index for the PS spheres were set at 1.59, which was provided by the manufacturer. The refractive index for GaN and aluminum were from RSoft, which sourced the information from Goldhahn and Rakic respectively [25,26]. At 370 nm, the refractive index of aluminum is 0.388 and its absorption coefficient is $1.47 \cdot 10^6$ cm^{-1}. Thickness of the GaN layer is set to be 0.1 μm and thickness of the aluminum varies depending on the simulation. All simulations used a Transverse Electric (TE) source set at the geometric center of the GaN layer.

4.2.1 Traditional Planar Structure

First, a planar structure of GaN on sapphire was simulated for reference. This structure has been well studied and due to the high refractive index of GaN, only a small percentage (~4-5%) of photons make it out to the surface. Figure 21 is a capture of the structure, with simulation

parameters described above. This structure was simulated, with the polar projection of its far-field intensity captured in Figure 22. As expected, the result is Lambertian as previously reported [1,4]. The extraction ratio calculated by the software was roughly 5.2%.

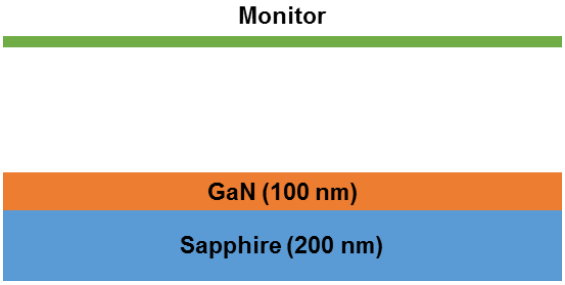

Figure 21 – Simulation of planar structure

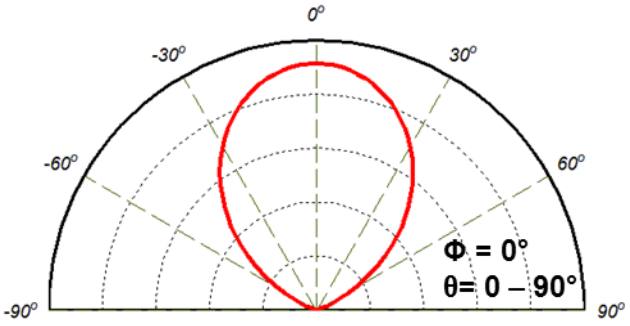

Figure 22 – Polar plot of far-field intensity of planar Structure.

4.2.2 Planar Structure with Nanospheres

Several simulations involving nanospheres were run for comparison with the planar structure. The structure is presented in Figure 23, with the spheres hexagonally packed to present the monolayer that would be on top of the GaN layer similar to those obtained in the experiments. Under the same conditions as the planar structure, the addition of 500 nm diameter PS sphere yielded the far-field intensity captured in Figure 24. The addition of the sphere has introduced a hexagonal pattern, with the maxima located at the center.

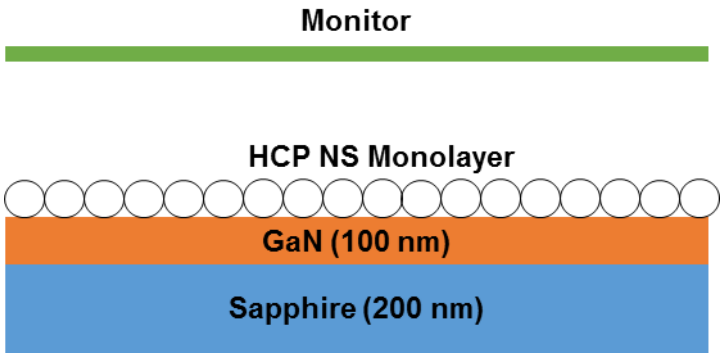

Figure 23 – Simulation profile with nanospheres.

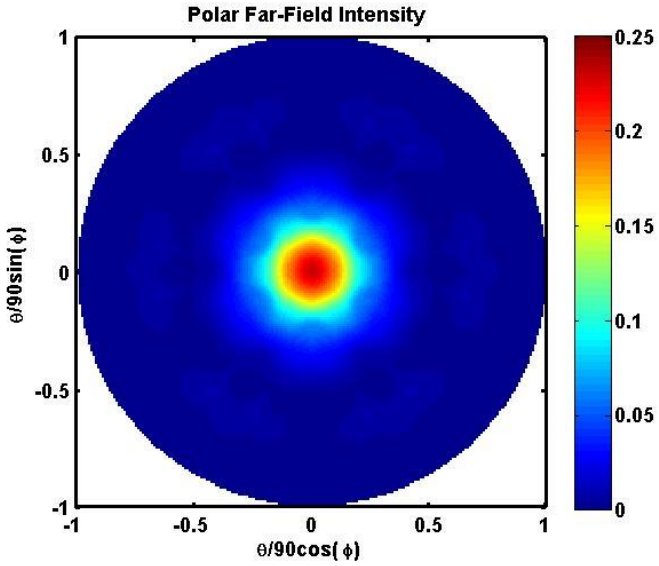

Figure 24 – Far-field intensity of structure with 500 nm PS spheres.

The effect of adding in the PS spheres can also be examined by looking at the intensity distribution from bird's eye view in Figure 25. It shows the spheres create a lobe of high intensity and webs that tapers out as the distance from the source increases. The image is annotated with the location of the spheres (outlined in white) that are in the center, noting that the higher intensity lobes line up with the center of the spheres radially, whereas the intensity along the line between the spheres decrease.

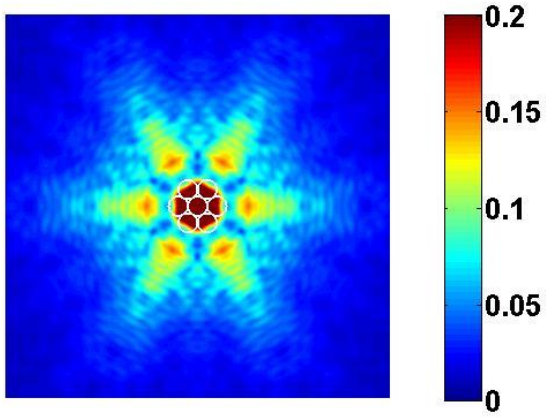

Figure 25 – Overhead view of electric field intensity.

To investigate the effect of different spheres that can be used, a scan was run with varying refractive index. Refractive index of 1 to 3 was run with a step size of 0.2 to generate Figure 26. Similar to previous studies, it shows that any sphere, as long as its refractive index is less than that of the GaN layer (in this case ~2.6), it will provide an enhancement due to reduction of Fresnel reflection. As the refractive index moves beyond that of GaN, the extraction ratio decreases since while it is providing enhancement, it is also trapping photons due to the higher refractive index.

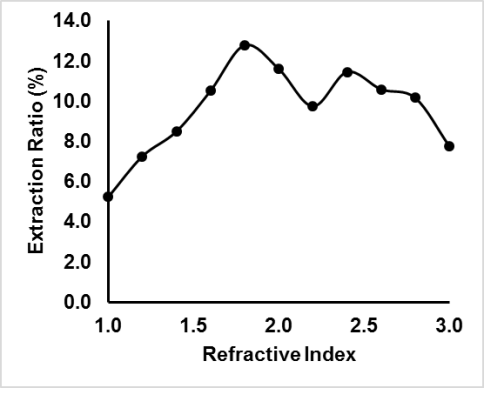

Figure 26 Extraction ratio versus refractive index of NS.

A sweep for various diameter spheres, which is much more tunable and controllable from a manufacturing perspective, was also run. This yielded an interesting result that peaks at roughly 650 nm diameter. A simulation issue of the results varying significantly depending on where the source is relative to the spheres was identified and care was taken to ensure that the excitation source is always in the center of a sphere. Figure 27 shows the plot of extraction ratio versus sphere diameter, showing enhancement upon the addition of nanospheres.

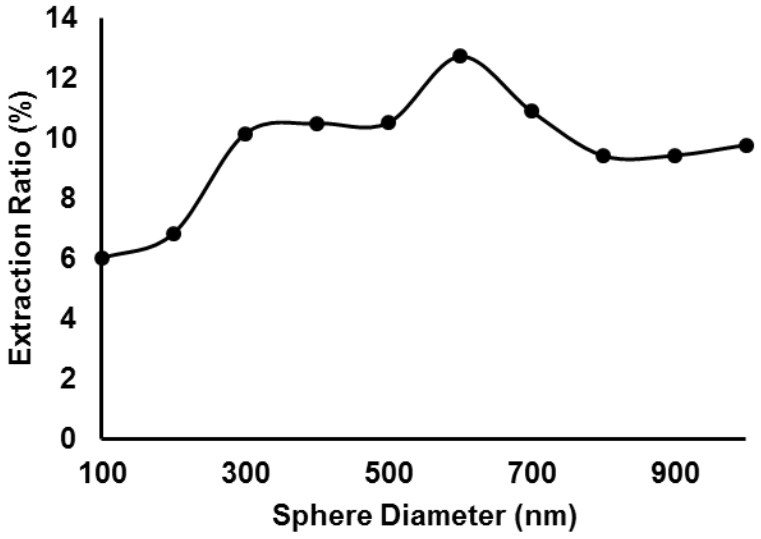

Figure 27 – Extraction ratio versus sphere diameter.

To mimic the possibility of what can experimentally be done, a sweep of varying sphere diameter was run, except this time with constant sphere spacing, essentially reproducing a mask with reduced diameter NSs. Starting with an initial diameter of 500 nm, a sweep down to 50 nm at 50 nm steps was done, with the resultant extraction ratio captured in Figure 28. As expected, the trend eventually decreases as the diameter reduces to almost zero, however not before it reaches a

peak at half of its original diameter, reaching an extraction ratio of 13.3%, which is a substantial increase and roughly a 2.5 times enhancement when compared with the planar structure.

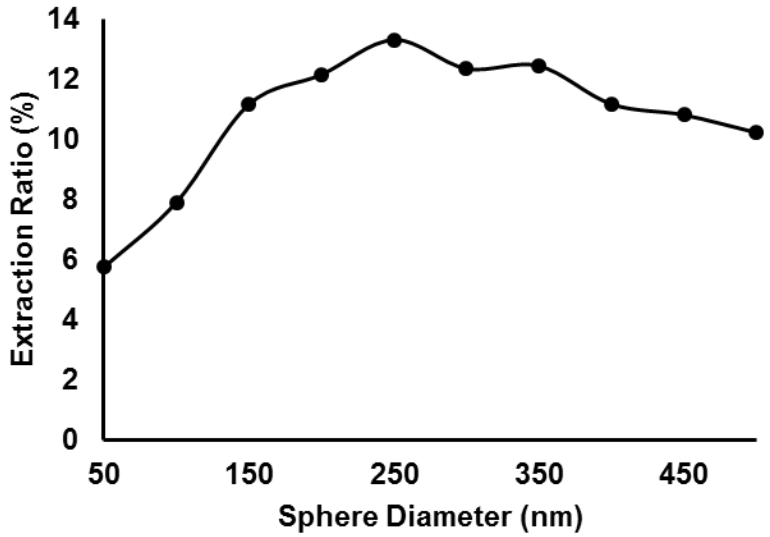

Figure 28 – Extraction ratio versus reduced sphere diameter with constant 500 nm spacing.

4.2.3 Planar Structure with Aluminum Structure

Various aluminums structure were simulated in an attempt to utilize LSPR for an enhancement over the UV spectrum, starting with the structure presented in Figure 29.

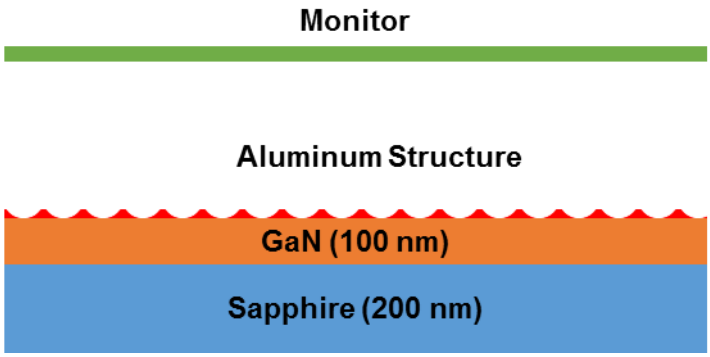

Figure 29 – Simulation profile 1 of aluminum structure on top of planar structure.

In this first profile, the aluminum NPs are simulated as 3-dimensional quasi-triangles that varies in height depending on the region of the nanoparticle. With an Al thickness of 25 nm, an enhancement of roughly 1.3 times was obtained. The enhancement is definitely due to the aluminum structure as a planar structure with 25 nm thick aluminum exhibits virtually no extraction. Upon comparing with literature, it's noted that although the angle of the sidewalls of the NPs are not 90°, they do not reach completely underneath the NSs as the first profile assumes. In order to replicate the structure more accurately, the spherical cavities were offset (Figure 30) and additional simulations were run. The resulting structure yielded no enhancement, which alongside the increased enhancement seen with an increased aluminum thickness in profile 1 (which increases the surface roughness), it's fair to conclude that the enhancement observed is most likely not due to LSPR.

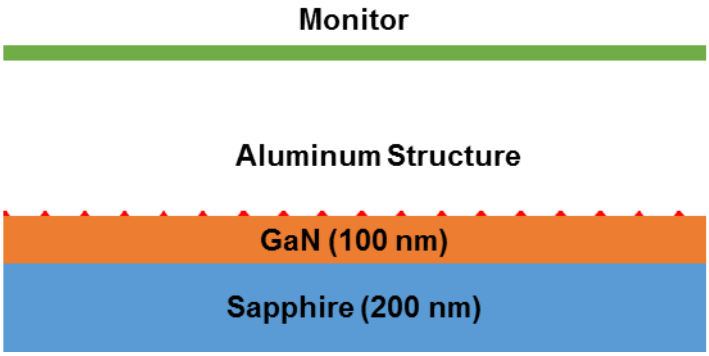

Figure 30 – Simulation profile 2 with aluminum structure.

A third simulation profile was attempted to model the NPs. Neglecting the angle of the sidewall, a HCP array of cylinders was used as the mask instead of a sphere, producing NPs with flat top surface. Simulation across three wavelengths were run with various reduced diameter sizes

and a constant spacing of 500 nm. No enhancement was exhibit in the shorter 280 nm and 370 nm wavelengths, which can be generated from AlGaN and GaN, respectively; however, enhancement was exhibited at 500 nm (InGaN).

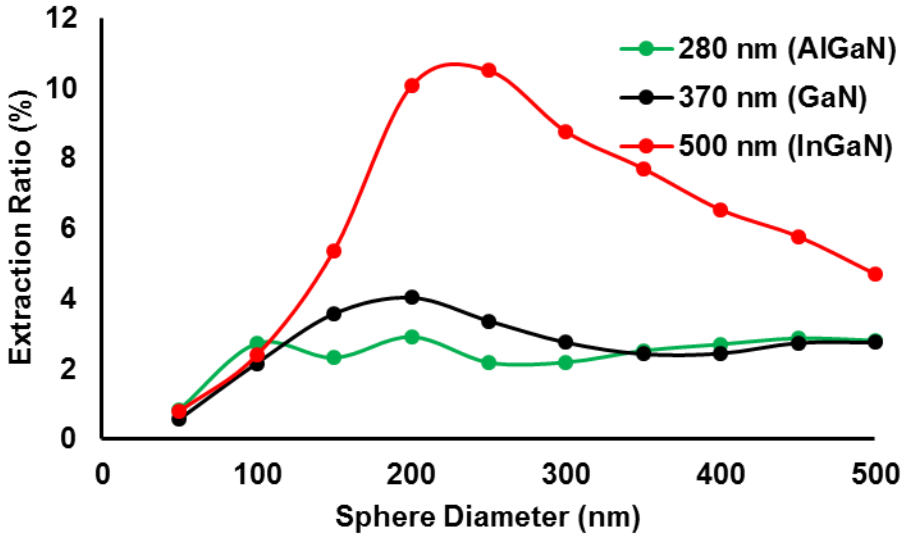

Figure 31 – Extraction ratio of aluminum profile 3 versus sphere diameter.

4.3 PL Measurements

A series of PL measurements were conducted to investigate the effects of NSL. The monolayer of PS spheres was deposited on GaN on double-side polished sapphire, which allowed the sample to be pumped from either the front or back. Their spectra were then measured for comparison. The control sample indicates no NSL performed, while the other two are two different samples (NSL1, NSL2) with 320 nm spheres on them. The ones with NSL match closely over all, while showing enhancement. The enhancement was much more apparent in the "defect" peak, due to either unintentional dopants or the sapphire substrate, which is present in Figure 33. Although the GaN substrate is said to be undoped, it's still unintentionally doped n-type with silicon. The

enhancement verifies the existence of the monolayer as it alters the spectrum significantly, on both of the samples with NSL performed.

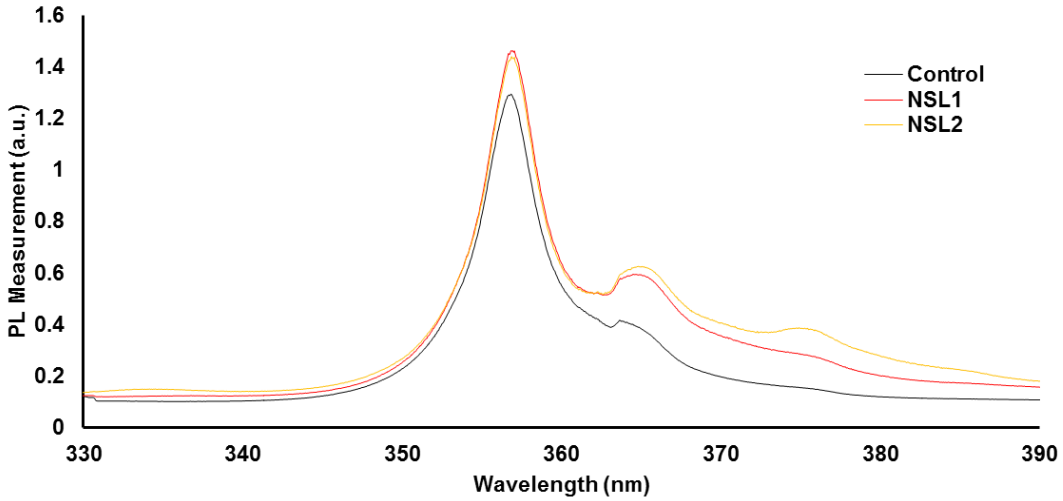

Figure 32 – PL measurement from 330 nm to 390 nm.

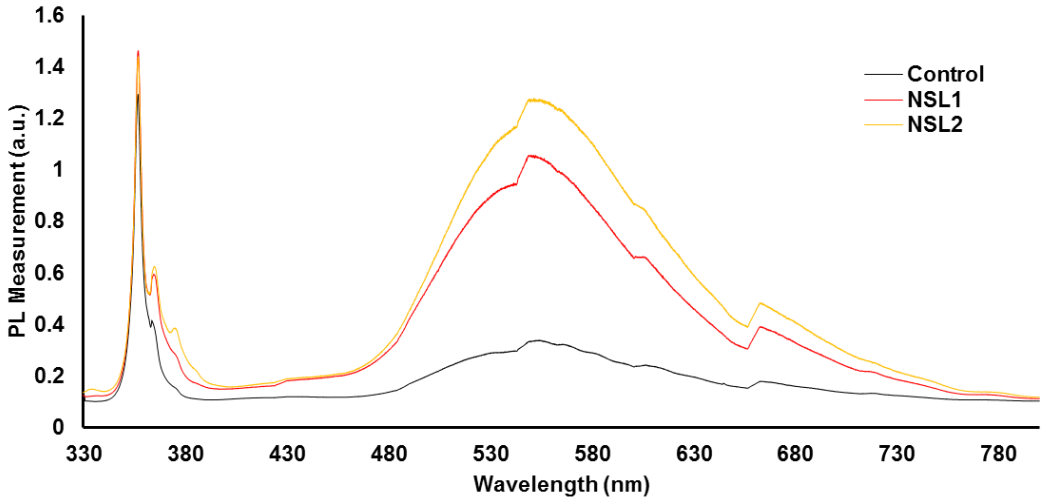

Figure 33 – PL measurement from 330 to 800 nm.

The multiple peaks around the 365 nm wavelength and the defect peak can also be due to the high power of the laser (~32 mW). Traditionally, only 5-6 mW is used and the higher power excites the electrons in higher energy levels.

4.4 Discussion

A series of experiments was run to produce and manipulate hexagonal masks for NSL. The experiment results showed promising masks, with confirmation of not only the hexagonal pattern, but also the possibility of extending such mask to large area, as those needed for actual devices. The subsequent steps after the deposition were also demonstrated and characterized to show successful reduction of sphere diameter down to 50 nm.

Both experimental and simulation results confirmed that the existence of nanospheres enhances the extraction ratio from the substrate. Simulation results also demonstrate that surface roughening produced by the masks enhance the UV spectrum. Several simulation models were developed to predict the possible behavior of localized surface plasmon, which appears to decrease top emission. Further investigation can be conducted to obtain more understanding of how the different sizes and shapes of NPs generated by NSL affect LSPR.

Chapter 5 Conclusion & Future Work

5.1 Conclusion

In this work, methods of performing NSL were surveyed, with two robust methods selected and performed to produce the HCP monolayer reliably. It was then followed by a sample of the different modifications, such as reduction of the sphere diameter, and deposition of metal, that can be done to produce various structures with small feature sizes without traditional patterning and lithography. The properties of the produced structures were characterized via PL measurement, which was compared to FDTD simulations to examine their effect on common optical structures, with the result being enhancement in the visible spectrum.

5.2 Future Work

In this section, additional experiments are outlined, with possible intended applications presented for further investigation of NSL.

5.2.1 Additional Experiments

Numerous experiments can be conducted to investigate nanosphere lithography further. The deposition of spheres can be performed on additional substrates, with different hydrophilicity. It has been shown that water plasma is effective in reducing the contact angle of GaN significantly, although the effect is not long term [21]. This is ideal as the adhesion between the monolayer and the substrate remains after the monolayer is initially deposited, and also due to the fact that the PS spheres only serve as a mask for additional processing steps. Experiments that increase the size of

the monolayer without sacrificing the quality should be conducted for manufacturability and integration purposes. Large-scale deposition is possible as formation of monolayers of over 4-inch diameter have been reported, and can possibly be transferred onto a substrate with great yield with a more refined experimental step [27]. There are also reports of two monolayer stacked on top of each other (double layer) being produced with NSL, which is also worthy of investigation [28].

Since GaN is a popular semiconductor material for various photonics devices, several other modifications to the substrate can be performed, such as producing nano-pillars or nano-cavities with the nanosphere mask to alter its optical properties. The resolution of such mask is only limited by the diameter of the spheres, which currently ranges from 100 nm to upwards of microns, made up of various material, such as SiO_2, TiO_2, *etc*. The effect of different material nanospheres have previously been investigated via simulation and they show the inclusion of the nanosphere layer in devices such as LEDs improves the device's efficiency [14].

5.2.2 Applications

The aforementioned nano-structures, with surface-plasmon also being one of them, and the nanospheres can be used to not only enhance the optical output of photonic devices, but they can also be used to alter the peak intensity and shift the output spectrum [16]. Combined with the usage of other metals besides aluminum, such as silver, specific ranges of the spectrum can be boosted. The generated mask and structures can be applied to not only LEDs, but also solar cells, to enhance their performance for further investigation of NSL [28-30].

Bibliography

[1] Y. K. Ee, "Reduced Dislocation Engineering and Enhanced Light Extraction Efficiency of III-Nitride Light Emitting Diodes," Ph.D. dissertation, electrical and computer engineering, Lehigh Univ., Bethelhem PA, 2010.

[2] P. Colson, C. Henrist, and R. Cloots, "Nanosphere Lithography : A Powerful Method for the Controlled Manufacturing of Nanomaterials," *Journal of Nanomaterials,* vol. 2013, 2013.

[3] K. A. Willets and R. P. Van Duyne, "Localized Surface Plasmon Resonance Spectroscopy and Sensing," *Annual Review of Physical Chemistry,* 2007.

[4] P. Zhu, G. Liu, J. Zhang, and N. Tansu, "FDTD analysis on extraction efficiency of GaN light-emitting diodes with microsphere arrays," *J. Disp. Technol.*, vol. 9, no. 5, pp. 317–323, 2013.

[5] S. Chuang and D. Wuu, "Plasmonic nanostructures for enhanced LED efficiency," SPIE Newsroom, doi:10.1117/2.1201009.001234.

[6] B. Kim, J. Bang, S. Jang, D. Kim, and J. Kim, "Surface texturing of GaAs using a nanosphere lithography technique for solar cell applications," *Thin Solid Films*, vol. 518, no. 22, pp. 6583–6586, 2010.

[7] L. Zhang and Y. Xiong, "Rapid self-assembly of submicrospheres at liquid surface by controlling evaporation and its mechanism," *Journal of Colloid and Interface Science*, vol. 306, pp. 428–432, 2007.

[8] E. M. Akinoglu, A. J. Morfa, and M. Giersig, "Nanosphere lithography – exploiting self-assembly on the nanoscale for sophisticated nanostructure fabrication," *Turkish Journal of Physics,* pp. 563–572, 2014.

[9] E. C. Brown, "Electrochemically Deposited Ceria Structures for Advanced Solid Oxide Fuel Cells," Ph.D. dissertation, department of electrical engineering, Caltech, Pasadena CA, 2011.

[10] J. Yu, L. Zheng, C. Geng, X. Wang, Q. Yan, X. Wang, G. Shen, and D. Shen, "Colloidal monolayer at the air / water interface : Large-area self-assembly and in-situ annealing," *Thin Solid Films*, vol. 544, pp. 557–561, 2013.

[11] J. C. Growth, R. Scholz, H. Jin, B. Fuhrmann, R. Scholz, F. Syrowatka, and A. Dadgar, "Fan , H . J . et al . Well-ordered ZnO nanowire arrays on GaN substrate fabricated via Well-ordered ZnO nanowire arrays on GaN substrate fabricated via nanosphere lithography," *Journal of Crystal Growth,* pp. 34–38, 2006.

[12] M. D. Malinsky, K. L. Kelly, G. C. Schatz, and R. P. Van Duyne, "Nanosphere Lithography : Effect of Substrate on the Localized Surface Plasmon Resonance Spectrum of Silver Nanoparticles," *Journal of Physical Chemistry B,* pp. 2343–2350, 2001.

[13] C. Haynes, T. R. Jensen, M. D. Malinsky, C. L. Haynes, and R. P. Van Duyne, "Nanosphere Lithography : Tunable Localized Surface Plasmon Resonance Spectra of Silver Nanoparticles," *Journal of Physical Chemistry B*, vol. 104, no. 45, pp. 10549–10556, 2000.

[14] P. Zhu, "Light Extraction and Nanomaterials for III-Nitride Based White Light-Emitting Diodes," Ph.D. dissertation, electrical and computer engineering, Lehigh Univ., Bethelhem PA, 2015.

[15] E. Hutter, B. E. Hutter, and J. H. Fendler, "Exploitation of Localized Surface Plasmon Resonance," *Advanced Materials*, October 2004, 2016.

[16] K. Huang, N. Gao, C. Wang, X. Chen, J. Li, S. Li, X. Yang, and J. Kang, "Top- and bottom-emission-enhanced electroluminescence of deep-UV light-emitting diodes induced by localised surface plasmons," *Scientific Reports,* vol4, 2014.

[17] F. Liu, W. Xie, Q. Xu, Y. Liu, and K. Cui, "Plasmonic Enhanced Optical Absorption in Organic Solar Cells With Metallic Nanoparticles Plasmonic Enhanced Optical Absorption in Organic Solar Cells With Metallic Nanoparticles," *Optics Express,* vol. 5, no. 4, 2013.

[18] V. Marrocco, M. Grande, R. Marani, G. Calò, V. Petruzzelli, and A. D. Orazio, "Plasmonic Nanostructures for Enhanced Light Concentration Devoted to Photovoltaic Applications,"

2010 12th International Conference on Transparent Optical Networks, Munich, 2010, pp. 1-4.

[19] Polyscience Inc., "Microspheres & Particles Handling Guide," [online], Available: http://www.polysciences.com/skin/frontend/default/polysciences/pdf/Microparticles%20Guide.pdf.

[20] J. Rybczynski, U. Ebels, M. Giersig, "Large-scale, 2D arrays of magnetic nanoparticles," *Colloids and Surfaces A: Physicochemical and Engineering Aspects*, Volume 219, Issues 1–3, 19 June 2003, Pages 1-6,

[21] J. Yeo and N. Kim, "Universal Surface Hydrophilicity Obtained by Using Low-temperature Plasma Treatment with H_2O gas for Nanosphere Lithography," *Journal of Korean Physics Society,* vol. 58, no. 1, pp. 1–4, 2011.

[22] Synopsys, "RSoft." https://optics.synopsys.com/rsoft/.

[23] M. D. Ionita, D. Kontziampasis, B. Mitu, A. Smyrnakis, E. Gogolides, and G. Dinescu, "Management of polymeric spheres diameter in colloidal lithography by low and atmospheric pressure plasma treatments," *Proc. International Conference on Phenomena in Ionized Gases,* 2015.

[24] A. Florio and P. K. Mohseni, "NSL Patterned Aluminum Deposition on Silicon," unpublished, RIT, Rochester NY, 2016.

[25] R. Goldhahn, K. Lange, and M. Feneberg, "Optical properties and band structure of highly-doped gallium nitride," *Proc. SPIE*9363, Gallium Nitride Materials and Devices X, 93630G (March 13, 2015).

[26] A. D. Rakic, A. B. Djuris, J. M. Elazar, and M. L. Majewski, "Optical properties of metallic films for vertical-cavity optoelectronic devices," *Applied Optics,* vol. 37, no. 22, pp. 5271–5283, 1998.

[27] J. Choi, "Development of Nanosphere Lithography Technique with Enhanced

Lithographical Accuracy on Periodic Si Nanostructure for Thin Si Solar Cell Application," Ph.D. dissertation, dept. of electrical engineering, ASU, Tempe AZ, 2015.

[28] X. Gu, T. Qiu, W. Zhang, and P. K. Chu, "Light-emitting diodes enhanced by localized surface plasmon resonance," *Nanoscale Research Letters,* pp. 1–12, 2011.

[29] B. Roberts, C. Science, and A. Arbor, "Broadband characteristics of surface plasmon enhanced solar cells," *Procs. IEEE Photovoltaic Specialists Conference,* pp. 2952–2954, 2010.

[30] J. Min Lee, J. Yi, W. Woo Lee, H. Yong Jeong, T. Jung, Y. Kim, and W. Il Park, "ZnO nanorods-graphene hybrid structures for enhanced current spreading and light extraction in GaN-based light emitting diodes," *Appl. Phys. Lett.*, vol. 100, no. 6, p. 061107, 2012.